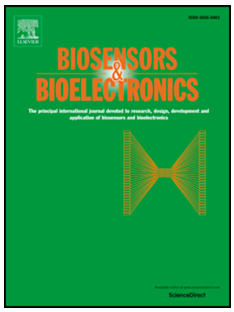

Picomolar detection of carbohydrate-lectin interactions on piezoelectrically printed microcantilever array

Oren Cooper, Hoang-Phuong Phan, Tom Fitzpatrick, Toan Dinh, Han Huang, Nam-Trung Nguyen, Joe Tiralongo

PII: S0956-5663(22)00128-2

DOI: https://doi.org/10.1016/j.bios.2022.114088

Reference: BIOS 114088

To appear in: *Biosensors and Bioelectronics*

Received Date: 18 November 2021

Revised Date: 1 February 2022

Accepted Date: 8 February 2022

Please cite this article as: Cooper, O., Phan, H.-P., Fitzpatrick, T., Dinh, T., Huang, H., Nguyen, N.-T., Tiralongo, J., Picomolar detection of carbohydrate-lectin interactions on piezoelectrically printed microcantilever array, *Biosensors and Bioelectronics* (2022), doi: https://doi.org/10.1016/j.bios.2022.114088.

CRediT author statement

Oren Cooper: Investigation, Writing - Original Draft, Visualization, Formal analysis, Methodology, Conceptualization **Hoang-Phuong Phan:** Investigation, Visualization, Formal analysis, Methodology, Writing - Review & Editing **Tom Fitzpatrick:** Investigation, Methodology **Toan Dinh:** Investigation, Formal analysis **Han Huang:** Investigation **Nam-Trung Nguyen:** Resources, Writing - Review & Editing **Joe Tiralongo:** Conceptualization, Supervision, Methodology, Resources, Writing - Review & Editing

Picomolar Detection of Carbohydrate-Lectin Interactions on Piezoelectrically Printed Microcantilever Array

Oren Cooper[a], Hoang-Phuong Phan[b], Tom Fitzpatrick[c], Toan Dinh[d], Han Huang[e] Nam-Trung Nguyen[b], Joe Tiralongo[a*]

a Institute for Glycomics, Griffith University, Gold Coast Campus, QLD 4215, Australia

b Micro and Nanotechnology Centre, Griffith University, Nathan Campus, QLD 4111, Australia

c School of Environment and Science, Griffith University, Gold Coast Campus, QLD 4215, Australia

d School of Mechanical and Electrical Engineering, University of Southern Queensland, Springfield Campus, QLD, 4300

e School of Mechanical and Mining Engineering, University of Queensland, St Lucia Campus, QLD 4072, Australia

KEYWORDS *Chemical Vapor Deposition, 3(Glycidyloxypropyl)-trimethoxysilane, Glycomics, Microcantilever Array, Micro-electromechanical Systems, Self-assembled Monolayers.*

ABSTRACT: Recent advances in micro-electromechanical systems (MEMS) has allowed unprecedent perspectives for label-free detection (LFD) of biological and chemical analytes. Additionally, these LFD technologies offer the potential to design high resolution and high throughput sensing platforms, with the promise of further miniaturization. However, the immobilization of biomolecules onto inorganic surfaces without impacting their sensing abilities is crucial for designing these LFD technologies. Currently, covalent functionalization of self-assembled monolayers (SAMs) present promising pathways for improving assay sensitivity, reproducibility, surface stability and proximity of binding sites to the sensor surface. Herein, we investigate the use of chemical vapour deposition of 3-(glycidyloxypropyl)-trimethoxysilane (GOPTS) as a versatile SAM for the covalent functionalization of a SiO_2 microcantilever array (MCA) for carbohydrate-lectin interactions with picogram sensitivity. Additionally, we demonstrate glycan immobilization to MCA is feasible using traditional piezoelectric microarray printer technology. Given the complexity of the glycome, the ability to spot samples in a high-throughput manner establishes our MCA as robust, label-free, and scalable means to analyze carbohydrate-protein interactions These findings demonstrate that GOPTS SAMs provide a suitable biofunctionalization route for MEMS and provides the proof of principle that can be extended to various LFD technologies toward a truly high-throughput and high-resolution platform.

INTRODUCTION

Biological detection and measurement systems, such as label-based arrays and label-free surface plasmon resonance are increasingly recognised as critical components of the drug discovery and development toolbox. In the last decade, novel micro-technologies such as Micro-Electromechanical Systems (MEMS) and micro-plasmonics systems have rapidly emerged, offering the potential for high-resolution, high-throughput label-free sensing of biological and chemical analytes. Both these platforms have been used to show antigen-antibody interactions,[1, 2] protein-protein binding,[3, 4] DNA hybridization,[5-7] and carbohydrate-protein interactions, [8-10] with unparalleled sensitivity. These studies provide the framework for the design of label-free detection (LFD) platforms that can allow for rapid screening, drug/pathogen binding kinetics, hit confirmation and/or receptor detection in biomedical research.

MEMS are promising candidates for LFD systems as they can provide quantitative measurements in small volumes of sample without the need for fluorescent, photochemical or radioisotope tags. For screening of large libraries, labelling is both expensive and limited by the size and position of the tag, which can limit the probes ability to target structures effectively.[11] Though this is not the case for LFD systems, they are still limited by surface functionalization of the inorganic/organic heterointerface. This process is crucial as it can directly influence the surface and interfacial energetics for both subsequent immobilization of functional biomolecules as well as the electronic [12] and plasmonic [13] properties of the heterostructure. Additionally, surface functionalization and biomolecule immobilization of microcantilevers lead to changes in surface stress that can induce defection of the mechanical element.[14] As such, careful attention to the fabrication of these devices is crucial for both sensitive and reproducible generation of binding events.

To address this, silane self-assembled monolayers (SAM) have been shown to generate inorganic/organic heterointerfaces suitable for biomolecule immobilization and LFD performance.[15-20] Here, alkoxy groups from organosilane molecules easily form SAMs on surfaces terminated with hydroxyl groups.[21] This can be easily achieved through oxygen (O_2) plasma cleaning on semiconductor surfaces such as gold (Au)[22], silicon (Si)[23] and silicon carbide (SiC).[24] Organosilane SAMs capable of specific biomolecule recognition have been generated through either chemical liquid deposition [25-28] or chemical vapor deposition (CVD).[29-33] Importantly, unlike liquid deposition techniques, which can result in the formation of multilayers with variable thickness and submicron aggregates or islands on

the material surface, CVD has been shown to be more reproducible and allows for nanometer thick organosilanes SAMs.[34, 35]

CVD is advantageous whenever it is necessary to coat irregular shapes, or channels in microfluidic devices as liquid coating is limited due to capillary forces. For MEMS, stiction from unintentional adhesion of microstructures to nearby interfacial forces such as water, van der Waals, chemical or electrostatic attractions are commonly cited as major failure points for microdevices.[36] Fortunately, organosilane SAMs represent promising anti-stiction coatings due to their low surface energy and low friction forces that significantly reduce adhesion in micro and nanostructures.[37, 38] Finally, the CVD of organosilanes generally only requires the silane itself in relatively small quantities (≤ 1 mL), and is therefore an affordable route for large scale functionalization. Taken together, this suggests that CVD organosilane coatings capable of biomolecule immobilization without affecting the inherent sensing ability of MEMS or plasmonic devices are crucial for the development of LFD biosensors.

We have previously shown that 3(Glycidyloxypropyl)-trimethoxysilane (GOPTS) SAMs are suitable for the functionalization of SiC films. Here, proof-of-principle using SiC microarray chips functionalized with GOPTS were compared to commercially available microarray surfaces.[39] Our GOPTS functionalized SiC revealed specific lectin-glycan interaction with similar signal intensities and decreased noise due to minimal non-specific interactions to the substrate. Additionally the I−V characteristics of SiC remained unchanged after silanization, implying that the chemical treatment in our GOPTS process did not alter the electrical properties of the SiC film.[39] Based on these findings, we sort to further investigate whether our GOPTS SAM is suitable to functionalize MEMS biosensors. Here, we report on the use of GOPTS SAMs to functionalize Si microcantilevers to provide the framework for the development of novel array-based LFD platforms. For the generation of a novel MCA, glycans as our model biomolecule were immobilized onto GOPTS-functionalized microcantilevers using standard piezoelectric microarray printer technology. Picogram detection of specific glycan-lectin interactions was confirmed through resonance frequency measurements and validated using COMSOL Multiphysics simulations.

MATERIALS AND METHODS

Microcantilever Array Functionalization

All chemicals unless specified were purchased from *Sigma-Aldrich*. Octosensis Microcantilever Arrays (Micromotive GmbH, Mainz, Germany) were O_2 plasma activated using a Tergeo plus Benchtop Plasma Cleaner *(PIE Scientific)* to allow covalent functionalization of GOPTS SAMs. The chamber was first purged and then left with O_2 (50 sscm) for 10 min before plasma was ignited at 100 RF for 15 min followed by a second O_2 purge for 10 min. The samples were carefully removed and quickly sealed to prevent dust contamination. CVD of GOPTS was performed in a B-580 Glass Titrator Oven (Büchi) as previously described.[39] In brief, a glass vial with 1 mL of GOPTS and 2% *N,N*-Diisopropylethylamine (DIPEA) was placed next to the MCA, to the back of the oven, away from the vacuum line. The oven was pressurized to 25 mmHg and heated to 150 °C to generate vapor. MCA were allowed to silanize overnight (16 hr). Subsequently, the oven was allowed to cool back to room temperature before being vented of any left-over methoxysilane. These microcantilevers were used in following experiments to determine whether GOPTS functionalization for biomolecule immobilization and detection is appropriate for MEMS.

Scheme 1: Synthesis route for GOPTS functionalization of SiO_2 microcantilevers. (1) CVD of GOPTS: 2% *N,N*-diisopropylethylamine in GOPTS, 25 mmHg, 150 °C, 16 h. (2) Aminated Glycan (either *N*-acetylglucosamine or mannose) is immobilized using a piezoelectric printer: overnight. (3) Epoxide neutralization to prevent ring closing: anhydrous methanol, acetic anhydride, 4 °C, 15 min. R group indicates position of acetyl moiety after acetylation.

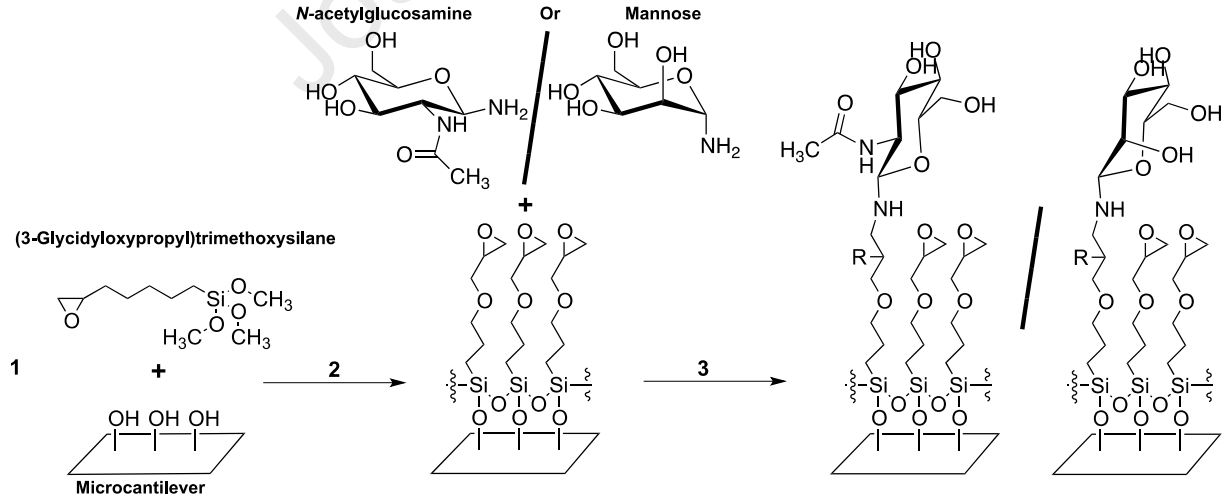

Holding Jig Fabrication

A Marathon Argus Inkjet Printer (Arrayjet, Roslin, UK), was used to robotically print onto the micro-cantilever array (MCA). This was originally designed to print microarrays using the dimensions of a laboratory slide. We customized the printer with a jig of equal dimension (75mm x 25mm) to enable printing onto MCA. The jig was fabricated out of 1.5 mm thick transparent cast acrylic sheet using a Trotec Speedy 300 (90-watt CO2 laser). The MCA was held in place inside of an engraved slot corresponding to its package outline. With this jig, the microcantilever placement was measured to be accurate to within 5 µm and precise to within 10 µm across the 3 jigs tested. A detailed approach presented in the Supporting Information, was

specifically employed so that the edges of the slot bed were kept vertical all the way down to the bottom of the slot bed, while the bed of the slot remained flat. This allowed for tight tolerances between the MCA and the jig.

Printing on Microcantilever Array

Using our MCA holding jig, a series of GOPTS functionalized MCAs were printed with either 1 mM Rhodamine B, α1-3-Mannobiose (Man-α1-3-Man) (Dextra, UK) or *N,N',N'',N'''*-Tetraacetyl chitotetraose ((GlcNAc-β1,4-GlcNAc)$_4$) (Dextra, UK) using the Marathon Argus Inkjet Printer (Arrayjet). For printing, glycans were amine functionalized as previously published by Day et al. (2009) [40] and suspended in 1:1 DMF:Dimethyl sulfoxide (DMSO) at a concentration of 500 µM. 200 pL of each glycans was piezoelectrically printed onto three separate cantilevers arrays, at 50% relative humidity at room temperature. Finally, printed glycan MCAs were carefully removed and sealed in a desiccator to prevent dust contamination. Printed MCAs are allowed to cure overnight to ensure the amine reacts with the open epoxide ring to form a secondary amine. Glycan MCAs were subsequently acetylated in 25% (v/v) acetic anhydride in methanol at 4 ˚C for 15 min, and then neutralized in 1:1 ethanolamine:DMF for 1 hr (see scheme 1). Here, unreacted epoxy rings are in a closed state and are unable able to react with acetic anhydride. On the other hand, acetylation of the free hydroxyl group of the opened epoxy ring is performed with acetic anhydride to prevent the epoxide ring opening in the presence of nucleophiles such as water. [39] Glycan MCAs were washed with 100% ethanol and then gently dried under vacuum. Fluorescent image acquisition of Rhodamine B printed microcantilevers was performed using an Innoscan 1100AL microarray scanner across the Cy3 channel. The printed microcantilevers was imaged using 5 mV laser power and 50% photomultiplier gain, in 5 µm steps, and image analysis was carried out using MAPIX (Innopsys) software.

Glycan Microcantilever Array Resonance Frequency Measurements

The resonance frequencies of each cantilever were monitored using a MSA-400 Laser Doppler Vibrometer (Polytec GmbH, Germany), in vacuum condition. [41] Measurement under vacuum reduces air damping, which enables the observation of resonant frequency of Si cantilevers self-actuated by their Brownian motion. The dynamic mode of MSA 400 was used to analyse the microcantilever beam under a continuous domain model. On separate microcantilevers, the resonance frequency of "unloaded" MCA after cleaning and GOPTS silanization, was compared. To confirm glycan-lectin interactions on our glycan MCA, we monitored the shift in resonance of the fundamental frequency on the same microcantilever over the course of experiment. Here, the resonant frequency of each microcantilever was measured after glycan printing. The shift in the resonant frequency can quantify the amount of glycan. Subsequently, the same MCA were blocked in 0.5 % BSA in 50 mM phosphate buffered saline (PBS), pH 7.4 for 5 min at RT. After washing with PBS, the glycan MCA were probed with wheat germ agglutinin (WGA, 1 µg) in 50 mM array PBS (PBS with 1.8 mM $MgCl_2$ and 1.8 mM $CaCl_2$), pH 7.4 containing 0.5 % BSA and allowed to hybridize for 15 min at RT. Following hybridization, MCAs were gently washed three times with 50 mM array PBS. Microcantilevers were allowed to dry under vacuum prior to resonant frequency measurements.

RESULTS AND DISCUSSION

Piezoelectric Printing on Microcantilever

Conventional biosensors require complex electronics interfacing, regular maintenance and extensive packing. MEMS technologies such as microcantilevers offer enormous potential for the detection of various analytes due to their high specificity, sensitivity, low cost and low analyte requirement.[42-46]. The generation of a MCA has yet to be realized due to the inability to specifically immobilize ligands in a high throughput manner. To provide the framework for a high throughput MCAs, we demonstrate the capacity of piezoelectric printing for functionalization of individual cantilevers. Designing based on commercially available microcantilevers, we developed a microarray slide holding jig that enabled direct printing on GOPTS-functionalized microcantilevers (*see Supporting Information Figure 1)*. To visualize successful printing and immobilization to the cantilever surface, we employed Rhodamine B as the printing biomaterial that allowed for fluorescent detection.

Here, the alignment of the microcantilevers using the holding jig is paramount, as cantilevers need to be aligned parallel to ensure printing on each individual cantilever. Using a conventional microarray scanner *(Figure 1A)*, the spot appears off centre. However, further visualization using fluorescence microscopy indicates the printed spots are well defined and deposited in the centre of the cantilever *(Figure 1B)*. The precise printing and alignment of Rhodamine B on Si cantilevers were possible due to the high resolution of the Marathon Argus printer (± 10 µm). The same method was applied to functionalize subsequent MCAs. Here, glycan immobilization was confirmed through optical microscopy *(see Supporting Information Figure 2)* as well as monitoring changes in resonance frequency.

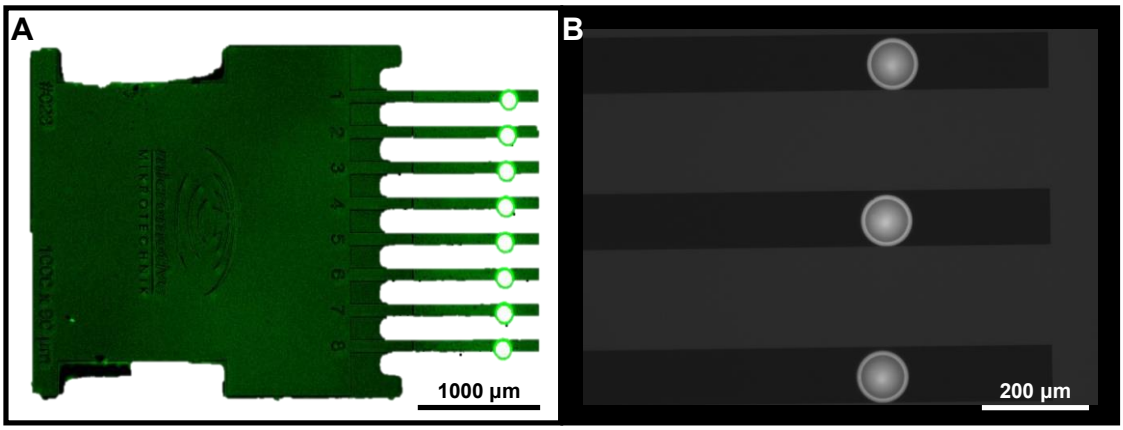

Figure 1: Piezoelectric printing of Rhodamine B onto Si microcantilevers. (A) Microarray scanner imaging of Rhodamine B printed microcantilevers; (B) Fluorescence microscopy imaging of Rhodamine B printed microcantilevers.

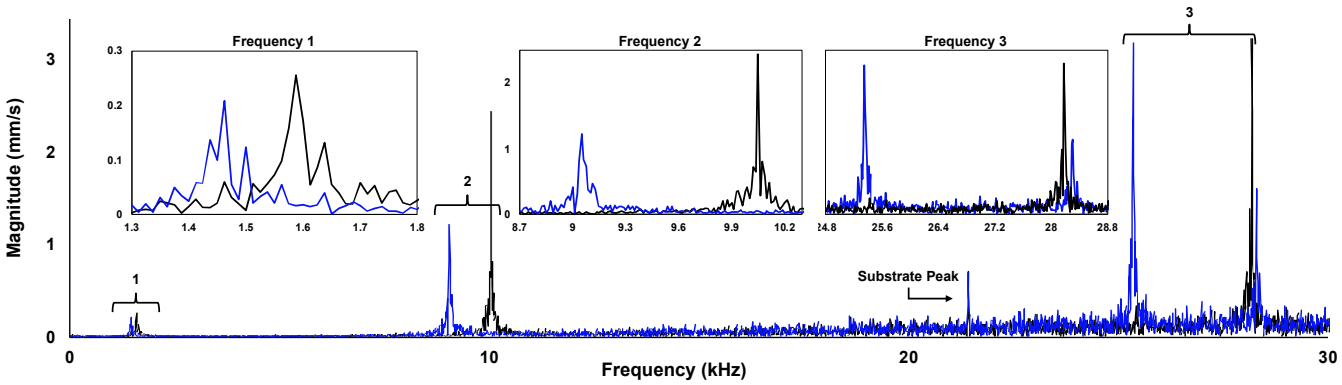

Figure 2: Representative frequency spectra of separate microcantilevers before (black) and after printing (blue). Unloaded microcantilever (black) Frequency 1: 1.5875 kHz (0.256 mm/s), Frequency 2: 10.05 kHz (2.436 mm/s), Frequency 3: 28.175 kHz (3.218 mm/s); Rhodamine B printed microcantilever (blue) Frequency 1: 1.4625 kHz (0.208 mm/s), Frequency 2: 9.05 kHz (1.216 mm/s), Frequency 3: 25.35 kHz (3.171 mm/s). Left shift of resonant frequency is indicated by black arrow.

Label Free Detection of Rhodamine B

To determine the effect that printing has on microcantilevers, the resonant frequency of unloaded and rhodamine B printed microcantilever was compared. Here, resonant frequency shifts were acquired from separate microcantilevers chips and as such are representative only. Nonetheless, informative qualitative data from changes in mass loading and surface stress can be monitored. Importantly, variations in the peak amplitude reflect minor changes in the position of the laser beam that leads to different angular motion read out. However. these changes do not affect resonant frequency on the spring constant (k), and the mass, (m). Finally, the substrate peak was monitored throughout the experiment to ensure the integrity of each array. Initial measurements on the unloaded microcantilever revealed three separate frequencies between 0 and 30 kHz, corresponding to the first three eigenmodes of resonance (*Figure 2*). We also observed a different mechanical response of another microcantilever printed with Rhodamine B. Here, the experimental results showed a left shift in all first three modes of the resonant frequencies. This left-shift is reasonable as the resonance frequency of an unloaded cantilever is given by:

$$f = \frac{1}{2\pi} \times \sqrt{\frac{k}{m}} \qquad (1)$$

where k, is the spring constant and m is the effective mass of the microcantilever. Printing the Rhodamine B onto the cantilever will increase total mass (m), leading to a decrease in the resonant frequency (unloaded frequency: 1.5875 kHz; Rhodamine loaded frequency: 1.4625 kHz). Additionally, as Rhodamine B was locally printed with only one spot of the cantilever, we assumed that no significant surface stress was induced from the bio-printing process and all changes in frequency can be directly attributed to mass loading. This was confirmed through calculation of the f1:f2:f3 ratios which were in good agreement with the theoretical ones, validating the accuracy of our measurements *(see Table 1)*.

Table 1: Comparison of theoretical and experimental cantilever vibration resonant frequency ratios.

Frequency	Experimental Ratio		Theoretical Ratio
	Unloaded	Rhodamine B	
f1:f2	6.33	6.19	6.27
f1:f3	17.75	17.33	17.55

Label Free Glycan Microcantilever Array

From our investigation of resonance frequency shifts due to GOPTS functionalization and Rhodamine B printing, we decided to use the fundamental frequency (the first mode resonant frequency of a vibrating object) to monitor changes in mass loading for a biologically relevant interaction. For proof-of-principle, we used well characterised glycan-lectin interactions to highlight the sensitivity of our MCA because these interactions are usually low affinity and due to labelling, inherently difficult to study.[47, 48] To quantitively detect glycan-lectin binding interactions as a function of mass, resonant frequency shifts from the same MCA were measured after glycan printing and after lectin (wheat germ agglutinin, WGA) hybridization.

Here α1-3-Mannobiose and *N,N',N'',N'''*-Tetraacetyl chitotetraose (hereafter referred to as (GlcNAc-β1,4-GlcNAc) were printed on alternate microcantilevers in triplicate. Figure 3A-B shows the frequency spectra of a α1-3-Mannobiose printed cantilever before (black) and after WGA hybridization (blue). No significant change in the resonant frequency was observed, indicating no interaction between the mannose coated cantilever and WGA. Figure 3C-D shows the response of the GlcNAc coated microcantilevers before and after WGA hybridization. The frequency spectra clearly show a left shift of the first mode frequency from 1.437kHz (before) to 1.343kHz (after hybridization). This result is consistent with our theoretical estimation, as WGA binds specifically to terminal *N*-acetylglucosamine and not to mannose terminated glycans.[49, 50] Taken together the detection of mass loading from only specific glycan-lectin interactions indicates successful immobilisation of functional glycans. For a rectangular-shaped cantilever, the loading mass (Δm) can be calculated from the change in the resonant frequency [51]:

$$\Delta m = \frac{k}{(2\pi)^2}\left(\frac{1}{f_1^2} - \frac{1}{f_0^2}\right) \qquad (2)$$

where f_0 is the initial fundamental frequency of glycan printed microcantilevers, and f_1 is the shift due to WGA interactions with glycan microcantilevers. Here, we used the spring constant provided by the manufacturer. Note that changes in spring constant can occur through absorbed molecules that may alter the cantilever stiffness or to changes in dimensions caused

by the interfacial organic layer.[54, 55] However, in our case, these influences are minimal assuming the SAM is evenly absorbed on the cantilever surface and does not affect the stiffness of the cantilever. In respect to MEMS, silane SAMs have demonstrated reduced adhesion and friction[54, 55] thereby improving performance and reliability. As previously demonstrated that CVD of our GOPTS monolayer is uniform [39], therefore adsorption induced changes in spring constant can be negligible. In addition, by printing on just the terminal end of the cantilever, the contribution from differential surface stress can be further minimized, as such resonant frequency can be mainly attributed to mass loading.[51] Taking these assumptions into consideration, we estimated the mass of a WGA binding across the three GlcNAc coated microcantilevers to be approximately 15.25 ± 6.88 pg (*see Supporting Information Table S2).*

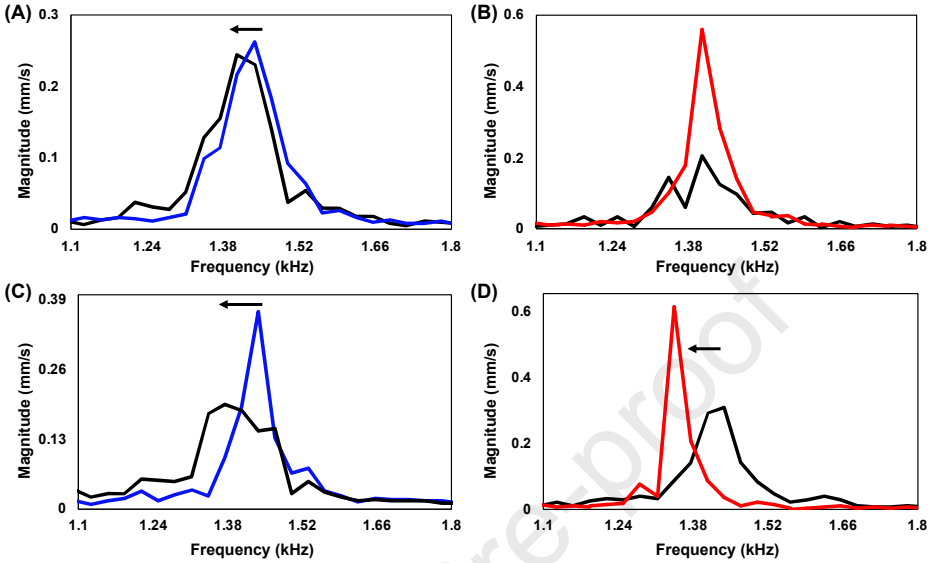

Figure 3: Representative frequency spectra of the microcantilevers after; GOPTS silanization (blue); Glycan Printing (black); WGA Hybridization (red). (A) Microcantilever after GOPTS silanization (blue), Frequency: 1.4375 Khz (0.263 mm/s) and subsequent α1-3-Mannobiose printing (black), Frequency: 1.40625 Khz (0.244 mm/s); (B) α1-3-Mannobiose printed microcantilever (black), Frequency: 1.40625 Khz (0.244 mm/s) and subsequent WGA hybridization (red), Frequency: 1.40625 Khz (0.560 mm/s); (C) Microcantilever after GOPTS silanization (blue), Frequency: 1.4375 Khz (0.368 mm/s) and subsequent GlcNAc printing Frequency: 1.375 Khz (0.196 mm/s), (D) GlcNAc printed microcantilever (black), Frequency: 1.4375 Khz (0.307 mm/s) and subsequent WGA hybridization (red), Frequency: 1.34375 Khz (0.613 mm/s). Left shift of resonance frequency is indicated by black arrow. Full resonance frequency spectrums are provided in the Supporting Information, Figure S3-6.

Table 2: Dimensions and Properties of the Microcantilever beam and Glycan object generated in COMSOL Multiphysics.

Dimensions/ Properties	Microcantilever (SiO_2)	Glycan (object)
Width	**9×10^{-5} m**	**9×10^{-5} m**
Length	**0.001 m**	**9×10^{-5} m**
Thickness	**1.1×10^{-6} m**	**1×10^{-7} m**
Volume	**-**	**$8.1\ 10^{-16}$ m^3**
Density	**2316 kg/m^3**	**Mass / volume ***
Young's Modulus	**165, 170, 175 GPa**	
Poisson's Ratio	**0.31**	

*Density was varied as a function of mass change

To confirm the results of the MCA resonant frequency measurements, simulation and eigenfrequency modelling were performed using COMSOL Multiphysics (5.6 Build 341). In the model, the cantilever was constrained at one end and freely suspended at the other end, Figure 4. The simulation was performed on a microcantilever beam with the dimensions and properties provided in *Table 1*, using a finite element model (FEMs). These dimensions were calculated in accordance to the manufacturer specifications. The Young's modulus (*E*) for Si was set at 165 – 175 GPa in our simulation as the (110) crystal orientation is preferred in most Si based resonators due to its large *E*. This range of *E* provided power to our simulation as FEMs are highly dependent upon the elastic modulus and thickness of the thin films [56, 57] The printed glycan was modelled by adding a mass (*as described in Table 1)* at a distance of 250 µm from the free end of the cantilever. To simplify our model the E and Poisson's ratio of our object was matched to Si. The density of the spot was varied by incrementally altering picogram mass on the cantilever and keeping the object volume constant. This ensured that changes to the eigenfrequency were directly attributed to mass loading on the microcantilever. To create an accurate model that best validates the printing data, we simulated a range of glycan mass' (10 – 20 pg, referred to hereafter as 'print'). The average eigenfrequency was calculated across the different E to create a model to simulate microcantilever printing (Table S1).This data was used to generate box and whisker plots of the eigenfrequencies to identify the model that best describes the E from our laser doppler vibrometer data.

To validate the picogram shifts in our experimental data due to lectin binding, an equivalent mass (as determined experimentally) was investigated. Here, a range of lectin probe mass (25 – 35 pg referred to hereafter as 'probe') were modelled at the various E (165, 170 and 175 GPa) and likewise plotted against our experimental data (*Figure 5*). Here, the results from the sim-

ulation for both the 'print' and 'probe' indicate that Si microcantilevers with an E of 175 GPa are the best model for our experimental data. Importantly this model relies on a range of 'print' and 'probe' picogram masses to best account for the experimental error from both glycan printing and subsequent lectin interactions to the printed MCA. Additionally, quantitative assessment of the data revealed no significant differences between the experimental results and all their respective simulated cantilevers as determined by two-way ANOVA ($P < 0.05$). Taken together this simulation validates our MCA resonant frequency changes which demonstrated picogram sensitivity for our carbohydrate-lectin interaction.

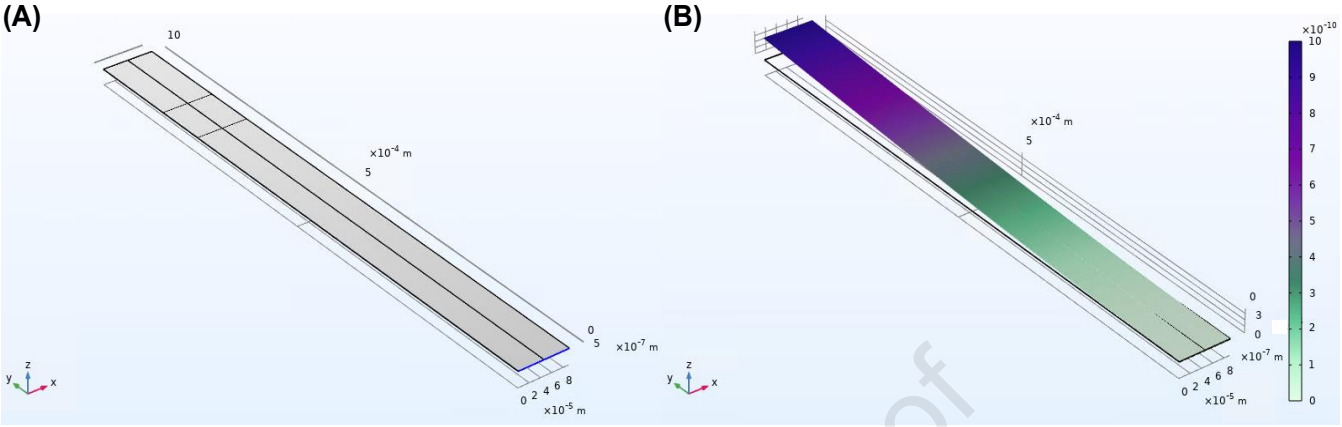

Figure 4: The view of the microcantilever using the structural mechanics application mode of MEMS module of COMSOL Multiphysics. (A) The generated microcantilever beam used to test the effect of mass loading on eigenfrequency. The printed spot area is indicated by the square and fixed end of the cantilever indicated in blue; (B) Example of eigenfrequency measurement readout, after COMSOL Multiphysics simulation. Here, the eigenfrequency of the uncoated microcantilever with an E of 165 GPa was determined to be 1448.4 Hz

Our results demonstrate the glycan MCA can reliably detect picomolar concentrations of WGA, while the sensor signal can be used to discriminate between specific glycan-lectin interactions. Our findings compare well with previous glycan microcantilever setups which have demonstrated high sensitivity and selectivity [8, 9]. In these reports, real-time measurements were performed on oligomannose cantilever sensors to detect either cyanovirin-N [8] or *Escherichia coli* strains with distinct mannoside binding properties.[9] In both instances the authors used an array of liquid-filled microcapillaries to functionalize microcantilevers with glycans and had to optimize exposure time to ensure maximum glycan deposition. Although highlighting the potential of real time LFD, the techniques employed were limited in their ability to generate high-throughput MCAs. Our work exemplifies the utility of non-contact piezoelectric printing for precise printing on to individual microcantilevers. Our method also provides the framework for label-free, high throughput glycan MCAs capable of picogram sensitivity.

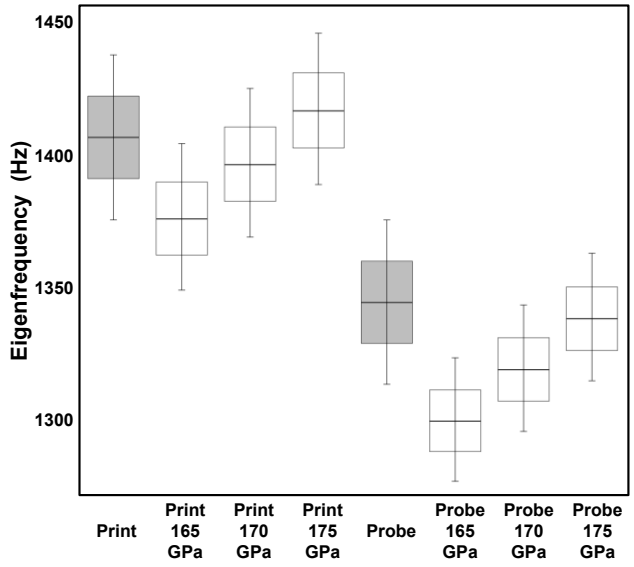

Figure 5: Box and whisker plot of experimental (grey) and simulation (white) data. Each simulation is grouped by their E (165, 170, 175 GPa) to determine the model that best explains our experimental microcantilevers. Non-significant differences between the experimental and simulated cantilevers were determined by two-way ANOVA ($P < 0.05$) followed by multiple pairwise comparisons with the Dunn's post-hoc test (due to unbalanced sample size) with p-values adjusted using the Bonferroni method. Normality and homoscedasticity assumptions were tested using Dago's test and Levene's tests ($P < 0.05$), respectively.

CONCLSUION

We present the framework and optimization of GOPTS SAMs for immobilization of the generation of novel glycan MCA. Here, GOPTS functionalisation route using CVD, enabled uniform deposition across the tested microstructures. Our work designing a glycan MCA, demonstrates for the first time that piezoelectric printing is a suitable route for the realisation of a high throughput LFD platform. We have shown proof-of-principle of a glycan functionalised array of individual microcantilevers to probe specific lectin interactions, with picomolar sensitivity. Importantly our approach using GOPTS SAMs and epoxide-based chemistry permits not only immobilisation glycans but also a variety of other biomolecules including proteins, antibodies and nucleic acids among others. More generally, this work demonstrates that CVD of silane SAMs represent a promising functionalisation route for next generation miniaturized self-sensing devices for a wide range of biomolecules.

ASSOCIATED CONTENT

Supporting Information

The Supporting Information is available free of charge on the ACS Publications website.
Supporting Information for Publication (PDF)

Document contains methods for fabrication of microcantilever array holding jig, COMSOL Multiphysics Simulation data, Light microscopy images of immobilized glycans to microcantilever array and full resonance frequency spectrums.

AUTHOR INFORMATION

Corresponding Author

*Joe Tiralongo, Institute for Glycomics, Griffith University, Gold Coast Campus, QLD 4222, Australia, Tel: + 61 7 5552 7029; E-mail: j.tiralongo@griffith.edu.au
†If an author's address is different than the one given in the affiliation line, this information may be included here.

Author Contributions

The manuscript was written through contributions of all authors. OC wrote the initial draft of the paper, performed all the experiments, data analysis and generated the Figures. TF designed and fabricated the holding jig. OC and TF performed all the printing. HH was instrumental in the generation of resonance frequency measurements and analysis was performed by OC, HPP and TD. Simulations were performed by OC, and confirmed by HPP and TD. JT conceived, designed, coordinated and revised the paper. JT planned together with OC all experiments, and glycan array printing and data analysis aspect of the paper. All authors have given approval to the final version of the manuscript.

Funding Sources

Any funds used to support the research of the manuscript should be placed here (per journal style).

Notes

Any additional relevant notes should be placed here.

ACKNOWLEDGMENT

HPP acknowledges the research support from Australian Re-search Council (ARC) through the DECRA project DE200100238

ABBREVIATIONS

CVD, Chemical Vapor Deposition; GOPTS, 3(Glycidyloxypropyl)-trimethoxysilane; LFD, Label Free Detection; MCA, Microcantilever Array; MEMS, Micro-electromechanical Systems; SAM, Self-assembled Monolayers

REFERENCES

1. Hwang, K. S.; Lee, J. H.; Park, J.; Yoon, D. S.; Park, J. H.; Kim, T. S., In-situ quantitative analysis of a prostate-specific antigen (PSA) using a nanomechanical PZT cantilever. *Lab Chip* **2004,** *4* (6), 547-52.
2. Arntz, Y.; Seelig, J. D.; Lang, H. P.; Zhang, J.; Hunziker, P.; Ramseyer, J. P.; Meyer, E.; Hegner, M.; Gerber, C., Label-free protein assay based on a nanomechanical cantilever array. *Nanotechnology* **2003,** *14* (1), 86-90.
3. Nugaeva, N.; Gfeller, K. Y.; Backmann, N.; Lang, H. P.; Duggelin, M.; Hegner, M., Micromechanical cantilever array sensors for selective fungal immobilization and fast growth detection. *Biosens Bioelectron* **2005,** *21* (6), 849-56.
4. Lee, J. H.; Yoon, K. H.; Hwang, K. S.; Park, J.; Ahn, S.; Kim, T. S., Label free novel electrical detection using micromachined PZT monolithic thin film cantilever for the detection of C-reactive protein. *Biosens Bioelectron* **2004,** *20* (2), 269-75.
5. Mukhopadhyay, R.; Lorentzen, M.; Kjems, J.; Besenbacher, F., Nanomechanical sensing of DNA sequences using piezoresistive cantilevers. *Langmuir* **2005,** *21* (18), 8400-8.
6. Hansen, K. M.; Ji, H. F.; Wu, G.; Datar, R.; Cote, R.; Majumdar, A.; Thundat, T., Cantilever-based optical deflection assay for discrimination of DNA single-nucleotide mismatches. *Anal Chem* **2001,** *73* (7), 1567-71.
7. Han, S.; Soylu, M. C.; Kirimli, C. E.; Wu, W.; Sen, B.; Joshi, S. G.; Emery, C. L.; Au, G.; Niu, X.; Hamilton, R.; Krevolin, K.; Shin, W.-H.; Shin, W. T., Rapid, label-free genetic detection of enteropathogens in stool without genetic isolation or amplification. *Biosensors and Bioelectronics* **2019,** *130*, 73-80.
8. Gruber, K.; Horlacher, T.; Castelli, R.; Mader, A.; Seeberger, P. H.; Hermann, B. A., Cantilever array sensors detect specific carbohydrate-protein interactions with picomolar sensitivity. *ACS Nano* **2011,** *5* (5), 3670-8.
9. Mader, A.; Gruber, K.; Castelli, R.; Hermann, B. A.; Seeberger, P. H.; Radler, J. O.; Leisner, M., Discrimination of Escherichia coli strains using glycan cantilever array sensors. *Nano Lett* **2012,** *12* (1), 420-3.
10. Gorelkin, P. V.; Erofeev, A. S.; Kiselev, G. A.; Kolesov, D. V.; Dubrovin, E. V.; Yaminsky, I. V., Synthetic sialylglycopolymer receptor for virus detection using cantilever-based sensors. *Analyst* **2015,** *140* (17), 6131-6137.
11. Ramachandran, N.; Larson, D. N.; Stark, P. R.; Hainsworth, E.; LaBaer, J., Emerging tools for real-time label-free detection of interactions on functional protein microarrays. *FEBS J* **2005,** *272* (21), 5412-25.
12. Stutzmann, M.; Garrido, J. A.; Eickhoff, M.; Brandt, M. S., Direct biofunctionalization of semiconductors: A survey. *physica status solidi (a)* **2006,** *203* (14), 3424-3437.
13. Spackova, B.; Wrobel, P.; Bockova, M.; Homola, J., Optical Biosensors Based on Plasmonic Nanostructures: A Review. *Proceedings of the IEEE* **2016,** *104* (12), 2380-2408.
14. Ibach, H., The role of surface stress in reconstruction, epitaxial growth and stabilization of mesoscopic structures. *Surface Science Reports* **1997,** *29* (5-6), 195-263.
15. Gfeller, K. Y.; Nugaeva, N.; Hegner, M., Rapid biosensor for detection of antibiotic-selective growth of Escherichia coli. *Appl Environ Microbiol* **2005,** *71* (5), 2626-31.
16. Campbell, G. A.; Mutharasan, R., Detection of pathogen Escherichia coli O157:H7 using self-excited PZT-glass microcantilevers. *Biosens Bioelectron* **2005,** *21* (3), 462-73.
17. Teixeira, S.; Burwell, G.; Castaing, A.; Gonzalez, D.; Conlan, R. S.; Guy, O. J., Epitaxial graphene immunosensor for human chorionic gonadotropin. *Sensors and Actuators B: Chemical* **2014,** *190*, 723-729.
18. Fradetal, L.; Stambouli, V.; Bano, E.; Pelissier, B.; Choi, J.; Ollivier, M.; Latu-Romain, L.; Boudou, T.; Paintrand, I., *Bio-Functionalization of Silicon Carbide Nanostructures for SiC Nanowire-Based Sensors Realization*. 2014; Vol. 14, p 3391-7.
19. Stambouli, V.; Ternon, C.; Serre, P.; Fradetal, L., Functionalization of Si-Based NW FETs for DNA Detection. *Nanos Nanotechno Ser* **2014**, 25-41.
20. Fradetal, L.; Bano, E.; Attolini, G.; Rossi, F.; Stambouli, V., A silicon carbide nanowire field effect transistor for DNA detection. *Nanotechnology* **2016,** *27* (23), 235501.
21. Ulman, A., *Ultrathin organic films*. Academic Press: Boston, 1991.
22. Fuchs, P., Low-pressure plasma cleaning of Au and PtIr noble metal surfaces. *Appl Surf Sci* **2009,** *256* (5), 1382-1390.
23. Martinet, C.; Devine, R. A. B.; Brunel, M., Oxidation of crystalline Si in an O2 plasma: Growth kinetics and oxide characterization. *J. Appl. Phys.* **1997,** *81* (10), 6996-7005.
24. Williams, E.; Davydov, A.; Motayed, A.; Sundaresan, S.; Bocchini, P.; Richter, L.; Stan, G.; Steffens, K.; Zangmeister, R.; Schreifels, J.; V. Rao, M., *Immobilization of streptavidin on 4H-SiC for biosensor development*. 2012; Vol. 258, p 6056-6063.
25. Koyano, T.; Saito, M.; Miyamoto, Y.; Kaifu, K.; Kato, M., Development of a Technique for Microimmobilization of Proteins on Silicon Wafers by a Streptavidin-Biotin Reaction. *Biotechnol Progr* **1996,** *12* (1), 141-144.
26. Ercole, C.; Del Gallo, M.; Mosiello, L.; Baccella, S.; Lepidi, A., Escherichia coli detection in vegetable food by a potentiometric biosensor. *Sensors and Actuators B: Chemical* **2003,** *91* (1-3), 163-168.
27. Awsiuk, K.; Bernasik, A.; Kitsara, M.; Budkowski, A.; Petrou, P.; Kakabakos, S.; Prauzner-Bechcicki, S.; Rysz, J.; Raptis, I., Spectroscopic and microscopic characterization of biosensor surfaces with protein/amino-organosilane/silicon structure. *Colloids Surf B Biointerfaces* **2012,** *90*, 159-68.
28. Schoell, S. J.; Sachsenhauser, M.; Oliveros, A.; Howgate, J.; Stutzmann, M.; Brandt, M. S.; Frewin, C. L.; Saddow, S. E.; Sharp, I. D., Organic functionalization of 3C-SiC surfaces. *ACS Appl Mater Interfaces* **2013,** *5* (4), 1393-9.

29. Yanni, Y.; Hosaka, T.; Miyake, T.; Zhang, G.-J.; Zako, T.; Funatsu, T.; Ohdomari, I., Preferential immobilization of biomolecules on silicon microstructure array by means of electron beam lithography on organosilane self-assembled monolayer resist. *Appl Surf Sci* **2004,** *234* (1-4), 102-106.
30. Takashi, T.; Takumi, H.; Takeo, M.; Yuzo, K.; Guo-Jun, Z.; Takashi, F.; Iwao, O., Hybridization of Deoxyribonucleic Acid and Immobilization of Green Fluorescent Protein on Nanostructured Organosilane Templates. *Japanese Journal of Applied Physics* **2005,** *44* (7S), 5851.
31. Zhang, G. J.; Tanii, T.; Zako, T.; Hosaka, T.; Miyake, T.; Kanari, Y.; Funatsu, T.; Ohdomari, I., Nanoscale patterning of protein using electron beam lithography of organosilane self-assembled monolayers. *Small* **2005,** *1* (8-9), 833-7.
32. Singh, J.; Whitten, J. E., Adsorption of 3-Mercaptopropyltrimethoxysilane on Silicon Oxide Surfaces and Adsorbate Interaction with Thermally Deposited Gold. *The Journal of Physical Chemistry C* **2008,** *112* (48), 19088-19096.
33. Oliveros, A.; Frewin, C. L.; Schoell, S. J.; Hoeb, M.; Stutzmann, M.; Sharp, I. D.; Saddow, S. E., Assessment of cell proliferation on 6H–SiC biofunctionalized with self-assembled monolayers. *J Mater Res* **2012,** *28* (1), 78-86.
34. Wang, Y., Vapor phase deposition of uniform and ultrathin silanes. *Proceedings of SPIE* **1998,** *3258* (1), 20-28.
35. Adamkiewicz, M.; O'Hara, T.; O'Hagan, D.; Hähner, G., A vapor phase deposition of self-assembled monolayers: Vinyl-terminated films of volatile silanes on silicon oxide substrates. *Thin Solid Films* **2012,** *520* (22), 6719-6723.
36. Tanner, D. M., Reliability of surface micromachined MEMS actuators. *22nd Int. Conf. Microelectronics* **2000**, 97-104.
37. Zhuang, Y. X.; Hansen, O.; He, J. C., Growth and properties of self-assembled monolayers on metals. *Journal of Physics: Conference Series* **2009,** *152*, 012029.
38. Zhuang, Y. X.; Hansen, O.; Knieling, T.; Wang, C.; Rombach, P.; Lang, W.; Benecke, W.; Kehlenbeck, M.; Koblitz, J., Vapor-Phase Self-Assembled Monolayers for Anti-Stiction Applications in MEMS. *Journal of Microelectromechanical Systems* **2007,** *16* (6), 1451-1460.
39. Cooper, O.; Phan, H. P.; Wang, B.; Lowe, S.; Day, C. J.; Nguyen, N. T.; Tiralongo, J., Functional Microarray Platform with Self-Assembled Monolayers on 3C-Silicon Carbide. *Langmuir* **2020,** *36* (44), 13181-13192.
40. Day, C. J.; Tiralongo, J.; Hartnell, R. D.; Logue, C. A.; Wilson, J. C.; von Itzstein, M.; Korolik, V., Differential carbohydrate recognition by Campylobacter jejuni strain 11168: influences of temperature and growth conditions. *PLoS One* **2009,** *4* (3), e4927.
41. Hu, Z.-W.; Wang, M.; Guo, C.-W.; Shan, Z.-W.; Li, J.; Han, W.-Z., Graphene-coated tungsten nanowires deliver unprecedented modulus and strength. *Materials Research Letters* **2019,** *7* (2), 47-52.
42. Lee, S. S.; White, R. M., Self-excited piezoelectric cantilever oscillators. *Sensors and Actuators A: Physical* **1996,** *52* (1-3), 41-45.
43. Wu, G.; Datar, R. H.; Hansen, K. M.; Thundat, T.; Cote, R. J.; Majumdar, A., Bioassay of prostate-specific antigen (PSA) using microcantilevers. *Nat Biotechnol* **2001,** *19* (9), 856-60.
44. Stevenson, K. A.; Mehta, A.; Sachenko, P.; Hansen, K. M.; Thundat, T., Nanomechanical Effect of Enzymatic Manipulation of DNA on Microcantilever Surfaces. *Langmuir* **2002,** *18* (23), 8732-8736.
45. Subramanian, A.; Oden, P. I.; Kennel, S. J.; Jacobson, K. B.; Warmack, R. J.; Thundat, T.; Doktycz, M. J., Glucose biosensing using an enzyme-coated microcantilever. *Appl Phys Lett* **2002,** *81* (2), 385-387.
46. Pei, J.; Tian, F.; Thundat, T., Glucose biosensor based on the microcantilever. *Anal Chem* **2004,** *76* (2), 292-7.
47. Kiessling, L. L.; Pohl, N. L., Strength in numbers: non-natural polyvalent carbohydrate derivatives. *Chemistry & Biology* **1996,** *3* (2), 71-77.
48. Collins, B. E.; Paulson, J. C., Cell surface biology mediated by low affinity multivalent protein–glycan interactions. *Current Opinion in Chemical Biology* **2004,** *8* (6), 617-625.
49. Lotan, R.; Sharon, N., The fluorescence of wheat germ agglutinin and of its complexes with saccharides. *Biochem Biophys Res Commun* **1973,** *55* (4), 1340-6.
50. Van Damme, E. J. M.; Peumans, W. J.; Pusztai, A.; Bardocz, S., *Handbook of Plant Lectins.* John Wiley & Sons: 1998; p 466.
51. Itoh, T., Scanning force microscope using a piezoelectric microcantilever. *Journal of Vacuum Science & Technology B: Microelectronics and Nanometer Structures* **1994,** *12* (3), 3618-3622.
52. Cherian, S.; Thundat, T., Determination of adsorption-induced variation in the spring constant of a microcantilever. *Appl Phys Lett* **2002,** *80* (12), 2219-2221.
53. Wachter, E. A.; Thundat, T., Micromechanical sensors for chemical and physical measurements. *Review of Scientific Instruments* **1995,** *66* (6), 3662-3667.
54. Srinivasan, U.; Howe, R. T.; Maboudian, R. In *Lubrication of Polysilicon Micromechanisms with Alkylsiloxane Self-Assembled Monolayers: Coefficient of Static Friction Measurements*, Tribology Issues and Opportunities in MEMS, Dordrecht, 1998//; Bhushan, B., Ed. Springer Netherlands: Dordrecht, 1998; pp 597-606.
55. Ashurst, W. R.; Yau, C.; Carraro, C.; Lee, C.; Kluth, G. J.; Howe, R. T.; Maboudian, R., Alkene based monolayer films as anti-stiction coatings for polysilicon MEMS. *Sensors and Actuators A: Physical* **2001,** *91* (3), 239-248.
56. Finot, E.; Passian, A.; Thundat, T., Measurement of Mechanical Properties of Cantilever Shaped Materials. *Sensors (Basel)* **2008,** *8* (5), 3497-3541.
57. Fang, W., Determination of the elastic modulus of thin film materials using self-deformed micromachined cantilevers. *Journal of Micromechanics and Microengineering* **1999,** *9* (3), 230-235.

Table of Contents

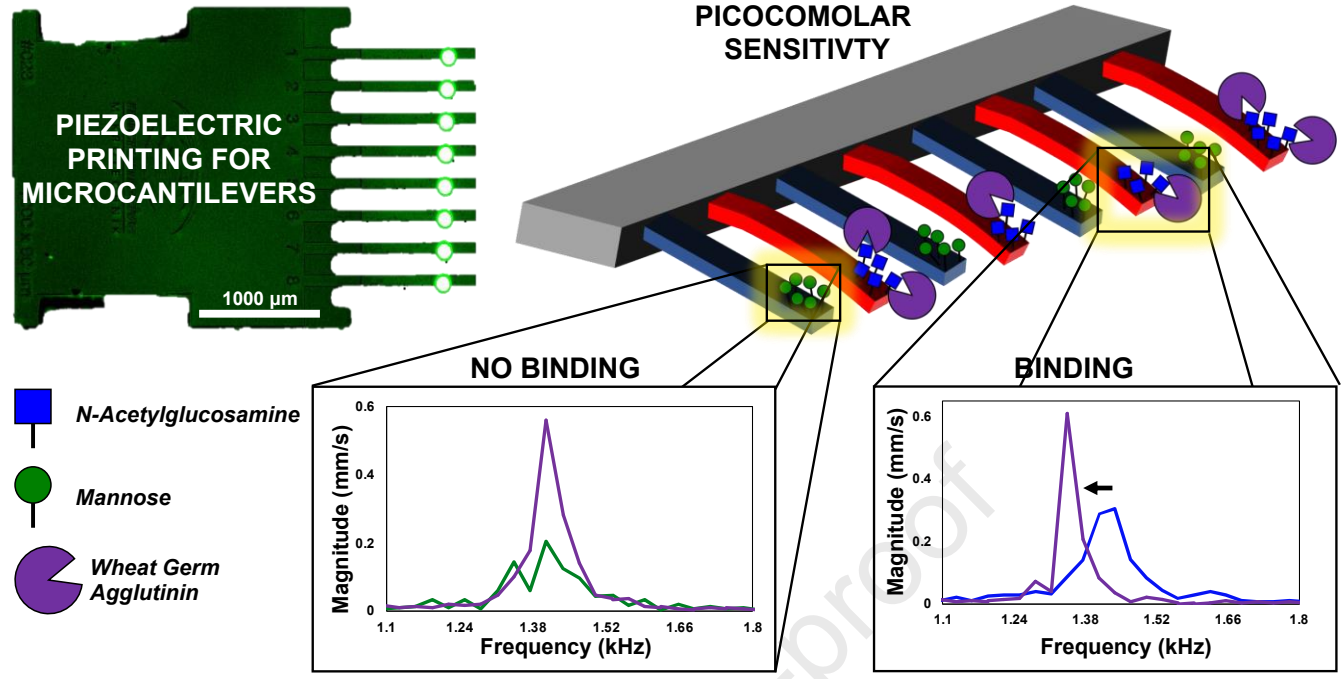

Highlights

Vapour deposition of silane self-assembled monolayers efficiently functionalizes MEMS

Piezoelectric printing can effectively immobilize biological samples onto microcantilever arrays

Label-free detection of specific carbohydrate-protein interactions with picomolar sensitivity

Microcantilever arrays are promising next generation miniaturized self-sensing devices

Declaration of interests

☒ The authors declare that they have no known competing financial interests or personal relationships that could have appeared to influence the work reported in this paper.

☐The authors declare the following financial interests/personal relationships which may be considered as potential competing interests: